Applied Catalysis B: Environmental 150–151 (2014) 57–62

Contents lists available at ScienceDirect

Applied Catalysis B: Environmental

journal homepage: www.elsevier.com/locate/apcatb

Engineering the TiO_2 outermost layers using magnesium for carbon dioxide photoreduction

Marta Manzanares[a], Cristian Fàbrega[a], J. Oriol Ossó[b,c], Lourdes F. Vega[b,c], Teresa Andreu[a,*], Joan Ramón Morante[a,d,*]

[a] Catalonia Institute for Energy Research, IREC, Jardins de les Dones de Negre 1, 08930 Sant Adrià de Besòs, Barcelona, Spain
[b] MATGAS Research Center, Campus UAB, 08193 Bellaterra, Spain
[c] Carburos Metálicos, Air Products Group, C/Aragón 300, Barcelona 08009, Spain
[d] Departament d'Electrònica, Universitat de Barcelona, Martí i Franquès, 1, 08028 Barcelona, Spain

ARTICLE INFO

Article history:
Received 7 October 2013
Received in revised form
18 November 2013
Accepted 20 November 2013
Available online 28 November 2013

Keywords:
Artificial photosynthesis
Carbon dioxide photoreduction
TiO_2 photocatalyst
Magnesium

ABSTRACT

Magnesium modified TiO_2 photocatalyst has been found to improve the CO_2 photoreduction reaction, with a high selectivity towards CH_4. Thus, Mg–TiO_2 has been synthesized with different compositions up to 2.0 wt%. Unlike the bare TiO_2, the surface reorganization originated by the presence of Mg enhances the formation of methane by a factor of 4.5, corroborating that complete reduction of CO_2 is achieved. It was found that the enhancement of the overall photocatalytic activity towards carbon dioxide reduction can be increased by a factor of 3, revealing a straightforward correlation with the surface states induced by the presence of the doping element. Finally, the evolution of the selectivity versus methane formation against hydrogen is discussed for the different magnesium loadings.

© 2013 Elsevier B.V. All rights reserved.

1. Introduction

The development of CO_2 capture and utilization technologies are an opportunity to use CO_2 as raw material and/or feedstock, not only for producing fine chemicals, but also to be recycled to fuels such as methane, carbon monoxide or methanol [1–3]. In 1979, Inoue and co-workers [4] demonstrated the photocatalytic conversion of carbon dioxide to organic compounds. Since then, the challenge of converting carbon dioxide to chemical energy using solar light is an attractive research field [5–8], contributing to the development of alternative technologies to the long-term storage of CO_2 in geological formations [9]. It is a clear and direct option for converting renewable energy to gas or even to liquid products [10–14].

Among all materials that have been reported for CO_2 photoreduction, TiO_2 has demonstrated to be one of the most promising due to its high stability, non-toxicity and low cost. However, semiconductors used as photocatalysts like TiO_2 presents some drawbacks that lead to low efficiencies of the CO_2 conversion to fuels: the fast recombination of the photo-induced holes (h^+) and electrons (e^-), and the requirement of ultraviolet (UV) irradiation due to their wide band gap. Different strategies have been addressed to overcome these two particular limitations and thus improve the photocatalytic activity of TiO_2 [15–19].

More recently, it has been shown by Chen [20,21] that solar absorption can be enhanced by introducing a controlled disorder in the surface layers of nanophase TiO_2 through hydrogenation. These authors proposed that the disorder-engineered TiO_2 nanocrystals exhibit substantial solar-driven photocatalytic activities, including the photo-oxidation of organic molecules in water and the production of hydrogen with the use of a sacrificial reagent.

Another important feature of the photocatalytic process concerns the kinetics of carrier's recombination. In this context, metals (e.g. Ag, Ru, Pt, Pd, Cu, etc.) have been also widely used to promote inhibition of charge recombination as they can act as electron traps [22]. Nonetheless and despite the relatively good performance of loading with noble metals at low concentration, their cost, availability and surface aggregation issues could limit its use and, hence, several alternatives are still under exploration [23–25].

Among them, alkali metals have been proposed to provide an effective way to induce changes in both electronic structure and surface states, as well as to promote the CO_2 adsorption [26]. Sodium, potassium, caesium and also some alkali earth metal like

* Corresponding authors at: Catalonia Institute for Energy Research, IREC, Jardins de les Dones de Negre 1, 08930 Sant Adrià de Besòs, Barcelona, Spain. Tel.: +34 933562615; fax: +34 933563802.
E-mail addresses: tandreu@irec.cat, tandrear@gmail.com (T. Andreu), jrmorante@irec.cat (J.R. Morante).

0926-3373/$ – see front matter © 2013 Elsevier B.V. All rights reserved.
http://dx.doi.org/10.1016/j.apcatb.2013.11.036

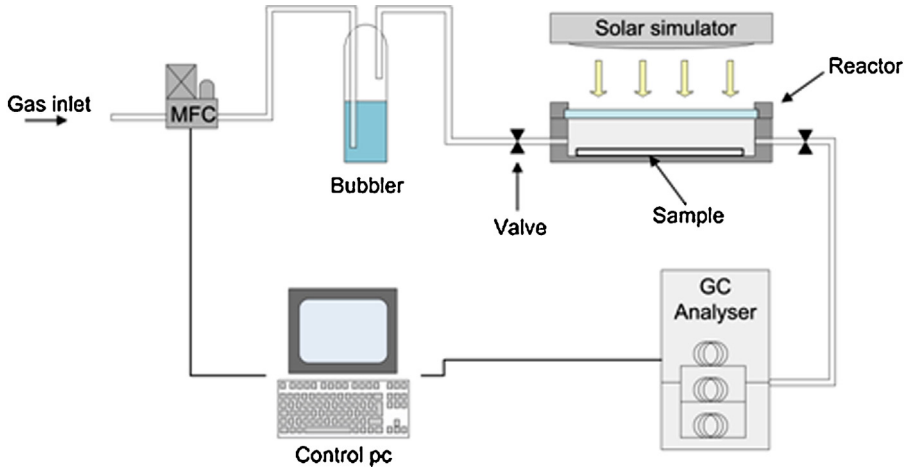

Fig. 1. Scheme of the experimental setup used for the evaluation of photocatalytic reduction of carbon dioxide.

calcium have been studied both, experimental and theoretically. However, magnesium doped TiO_2 has scarcely been reported and it has only been described for solid solution of both oxides [27,28]. To the best of our knowledge, magnesium doped TiO_2 has not been investigated as photocatalyst for the solar conversion of carbon dioxide to fuels assisted with water as hole scavenger although some paper reports on TiO_2:MgO heterostructures [29,30]. The interest on magnesium relies in its higher electronegativity and ionization energy, similar ionic radius [31] and reduced Lewis acid strength than Ti^{4+} [32], which in turns out in a modification of the surface acidic properties. These features result in the promotion of CO_2 chemisorption and, thus, enhancing the photocatalytic reaction. Furthermore, its low cost and toxicity, its properties and its relative high abundance (being the eighth most abundant element in the earth's crust) make it a suitable candidate for doping TiO_2 instead of other more expensive metals.

In spite of these promising characteristics, it should be remarked that the complementary effects of the modifications at the surface structure caused by the magnesium presence have been scarcely considered to date. The surface disorder and surface bonded groups may play a noteworthy role concerning the yield of photocatalytic reaction taking place at the surface, bearing in mind that outermost layers can determine the surface state density as well as the recombination kinetics of the photogenerated carriers.

In this paper, we present the photoreduction of carbon dioxide by magnesium doped TiO_2 with unprecedented selectivity towards CH_4. Mg–TiO_2 has been synthesized by a sol–gel method with several compositions up to a magnesium loading of 2.0% in weight. The detailed characterization of the induced surface modifications and their connection with the enhancement of the CO_2 photoreduction to CH_4, which is supported by the dependence of these surface states on the Mg concentration, as well as the relation of the effective overall photocatalytic productivity with the Ti^{3+} and non-lattice oxygen related states concentrations are revealed.

Finally, the evolution of the selectivity versus methane formation against hydrogen formation is discussed for the different magnesium loadings.

2. Experimental

2.1. Synthesis of doped titanium dioxide nanoparticles

The synthesis procedure was a modification of the previously reported for doped TiO_2 nanoparticles [33]. Briefly, a 0.5 M solution of titanium (IV) isopropoxide (Alfa Aesar, 97+%) in isopropanol (Panreac, QP) was added drop wise under stirring over DI water adjusted to pH 3 with HNO_3 (VWR, 69%), and kept under stirring overnight for a complete peptization. The white precipitate was collected by filtration and rinsed with pure water in order to remove the isopropanol solvent. The retrieved gel was suspended in DI water containing the required amount of magnesium nitrate hexahydrate (Alfa Aesar, ACS 98.0–102.0%), adjusted to pH 3 with HNO_3, transferred to a stainless steel Teflon-lined autoclave, and kept at 150 °C for 3 h under stirring. The resultant particles were collected, washed several times with DI water and dried in an oven at 80 °C. Finally, the resulting powder was calcined at 600 °C for 3 h.

2.2. Structural characterization

High resolution transmission electron microscopy (HRTEM) images were recorded with a JEOL JEM-2100 microscope. X-ray diffraction (XRD) analysis was performed using a PANalytical X'Pert PRO MPD Alpha1 powder diffractometer with monochromatized Cu Kα1 radiation working at 45 kV–40 mA in a Bragg Brentano configuration. X-ray photoelectron spectroscopy (XPS) experiments were performed in a PHI 5500 Multitechnique System (from Physical Electronics) with a monochromatic X-ray source (Al Kα 1486.6 eV energy and 350 W), placed perpendicular to the analyzer axis and calibrated using the $3d_{5/2}$ line of Ag with a full width at half-maximum (FWHM) of 0.8 eV. Details of the analysis of XRD patterns for calculating the crystal size and phase composition as well as the XPS analysis can be found in the Supplementary Data.

2.3. Photocatalytic activity towards carbon dioxide photoreduction

Due to the problem of the poor CO_2 solubility in liquid water, a gas–solid system was used to evaluate the capacity of the synthesized materials to reduce CO_2 into valuable byproducts. The photoreactor used was a stainless steel cylinder provided with an optical window made of borosilicate glass (Schott Borofloat® 33) having an internal volume chamber of 200 ml. 150 mg of the photocatalyst was immobilized on flat glass substrates (59 cm^2) by aerography using ethanol as solvent. Once deposited, the samples were dried overnight at 300 °C to ensure the complete removal of the solvent.

Fig. 1 illustrates the experimental setup used. The photoreactor was purged for 1 h with a constant flux (200 ml min^{-1}) of pure CO_2 (99.995%, Air Products) bubbled through water. After purging, inlet and outlet gas valves were closed and the reactor was illuminated remaining at atmospheric pressure. The radiation source was a 550 W Xe-lamp with a AM 1.5G filter (solar

Table 1
Phase composition, crystalline size and anatase cell parameter of Mg–TiO_2 samples (A: anatase; B: brookite; R: rutile).

Sample	Phase content (%)			Crystal size (nm)			Anatase
(% Mg)	A	R	B	A	R	B	*c* (nm)
0.0	85.1	2.6	12.3	30.7	44.0	10.7	0.949
0.2	88.5	0.6	11.5	24.1	35.0	13.0	0.933
0.5	84.2	–	15.8	13.5	–	10.4	0.939
1.0	83.5	–	16.5	13.1	–	9.6	0.947
2.0	87.1	1.7	11.2	21.8	14.7	11.0	0.955

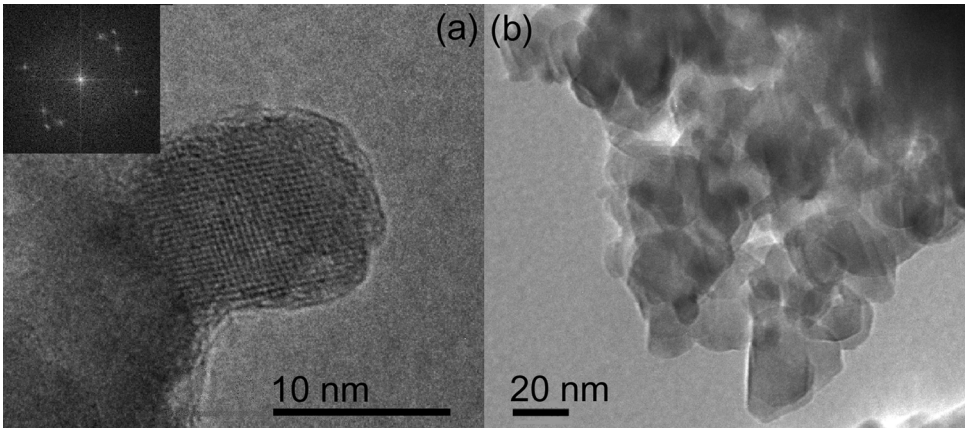

Fig. 2. HRTEM (a) and TEM (b) images of 0.2 wt% Mg-loaded catalyst.

simulator ABET Technologies, SUN2000) with a uniform illuminated area of $10 \times 10\,cm^2$, providing $100\,mW\,cm^{-2}$ in the work plane measured with a thermopile detector. During the experiment, the working temperature was stabilized at 33 °C by self-heating from the illumination source. After 3 h of irradiation, the gas phase was analyzed by gas chromatography (GC) using a multichannel Varian 490 microGC equipped with two Molsieve columns with argon carrier for hydrogen analysis and with helium carrier for methane and carbon monoxide analysis, to detect the main products of the photoreduction process.

Prior to photoreduction experiments, blank tests were performed. Samples were tested under humid argon (instead of CO_2) atmosphere to verify that no organic residues from the synthesis or from the immobilization procedure remained on the surface [34,35]. Results were near the limit detection and then considered as not significant.

3. Results and discussion

3.1. Structural characterization

The structural characterization of pure and magnesium doped titanium dioxide was investigated by means of X-ray diffraction (XRD), which are shown in the Supplementary Data (Fig. S1). All samples were mainly composed of anatase (JCPDS 84-1286), with a small fraction of brookite (JCPDS 29-1360) and a residual of rutile (JCPDS 73-1765). A phase segregation of $MgTiO_3$ (JCPDS 6-494) has also been observed, clearly considering the threshold detection resolution, at least for the highest loading of magnesium included in this study (2.0 wt% Mg), as it can be seen by the appearance of the peaks corresponding to this crystal structure at 2θ values of 32.9° and 35.5°. It is plausible to think that, for lower loading, its detection is out of the experimental resolution of the equipment, or it does not exist yet. In spite of the nano dimensional size of these particles, the main information obtained from XRD spectra is related to the bulk nanoparticle characteristics. The phase content and crystalline size of each titanium dioxide polymorph is shown in Table 1. Details of calculation can be found in the Supplementary Data. Additionally, transmission electron microscopy (TEM) images (Fig. 2) confirmed the crystallinity of the samples and the distribution of crystalline sizes compared with those calculated using the Scherrer equation. It can be observed that the crystalline size corresponding to the rutile phase diminished as the Mg loading was increased, suggesting an inhibition of the crystal growth because of the presence of magnesium. As a consequence, the rutile phase formation was also prevented or reduced until the segregation of Mg was clearly evident in form of $MgTiO_3$ for the highest loading sample. Accordingly, this inhibition on crystal growth is also affecting the anatase phase, broadening its diffraction peaks. These features indicate that magnesium is incorporated into the titania lattice and affects the crystal growth due to the formation of Ti—O—Mg bonds [28]. Since the atomic radius of magnesium is close to that of titanium, Mg^{2+} could substitute Ti^{4+} into the TiO_2 lattice. Nevertheless, the electrical neutrality condition requires a reduction around the neighbouring sites for compensating the unbalance of charge. This readjustment causes a lattice distortion that has been pointed out by the fine analysis of the anatase XRD peaks.

From lattice parameters of the anatase phase, it was revealed the existence of a lattice cell contraction in the bulk of the nanoparticles, mainly in the *c*-axis, by the incorporation of magnesium [36], while the *a* and *b* axes remained nearly constant around 0.378 nm (Table 1). This contraction exhibits a maximum for the lowest doping level and a relaxation of the structure with higher magnesium loading. The magnesium incorporation into the other phases was difficult to discern at these doping levels, since the isomorph $MgTi_2O_5$ also exist, with pseudobrookite structure, which can be further decomposed to $MgTiO_3$ and TiO_2 [37], hypothesis that is plausible since at 2.0 wt% $MgTiO_3$ is observed.

3.2. Outermost layer analysis

The surface chemical composition was examined by means of X-ray photoelectron spectroscopy (XPS). For all degrees of concentration, Mg *1s* peak was detected corroborating the presence of Mg atoms at least in the first 3–5 monolayers beneath the surface. The atomic concentrations of Mg, O and Ti at the surface were

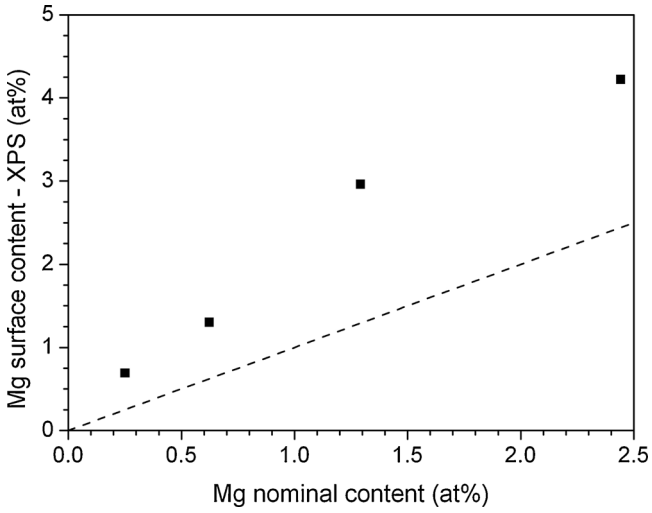

Fig. 3. Amount of Mg detected at the surface versus the nominal atomic concentration in the bulk. Dashed line represents the ratio 1:1.

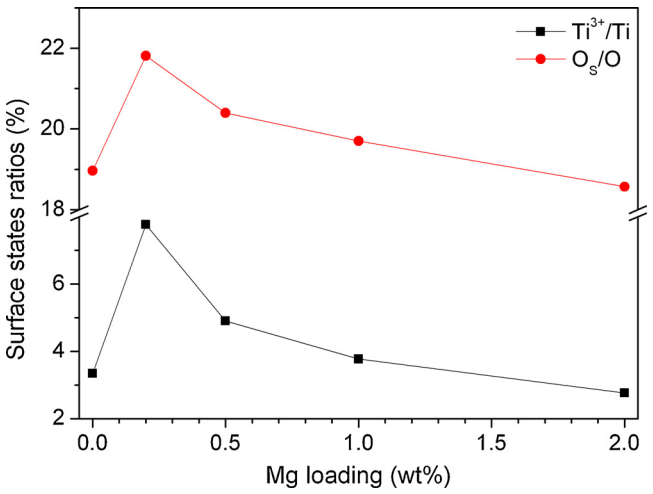

Fig. 4. Relative abundance of O_S and Ti^{3+} for pure and Mg-doped TiO_2 nanoparticles.

retrieved from Mg *1s*, O *1s* and Ti *2p* high resolution peaks of the spectra and then the atomic percentage were obtained. According to these results, shown in Fig. 3, there is a higher magnesium concentration at the surface than the nominal added value, suggesting a U-shape profile for magnesium ions inside the nanocrystals. These phenomena of surface segregation on TiO_2 nanoparticles have also been found for other additives [38,39]. This larger effective concentration near the surface is supported by the fact that we already found Mg segregation under $MgTiO_3$ at values as low as 2.0 wt%. However, before complete segregation, it has been observed that magnesium incorporation causes a highly distorted surface which is the main origin of the restriction on grain growth. As previously discussed in Section 3.1, magnesium ions, mostly accumulated at the surface, can substitute titanium ions in anatase phase and, consequently, the introduction of impurities to the TiO_2 promotes the formation of defects to compensate the charge. In the case of Mg, according the Kröger–Vink notation, the defective reaction caused by the Ti^{4+} substitution by Mg^{2+} can be expressed as follows:

$$MgO \xrightarrow{TiO_2} Mg''_{Ti} + O_O^X + V_O^{\bullet\bullet} \quad (1)$$

where Mg''_{Ti} indicates a Mg^{2+} in a Ti^{4+} lattice site; O_O^X represents a O^{2-} in a normal lattice site and $V_O^{\bullet\bullet}$ an ionized oxygen vacancy.

However, these ionized oxygen vacancies are not stable at the surface and they tend to neutralize either by the chemisorption of molecular oxygen, the formation of hydroxyl groups [40] or the reorganization of the crystalline structure by the creation of Ti^{3+} [41], giving the well know *n*-type behaviour to the defective TiO_2. Then, the presence of magnesium can cause a reorganization of the surface promoting a variety of chemical surface states which can be elucidated by examining the high resolution XPS spectra in Ti *2p* and O *1s* zones.

The Ti *2p* signal was deconvoluted in four different contributions (see Supplementary Data, Fig. S2b) attributed to the Ti^{4+} doublet (458.7 and 464.4 eV) and a minor doublet for Ti^{3+} (457.7 and 463.4 eV) [42], while the O *1s* peak (see Supplementary Data Fig. S2c) displayed a broader asymmetric spectra due to the contributions corresponding to different chemical states reported in the literature [43,44]: oxygen in TiO_2 lattice (O_L) (529.9 eV); chemisorbed oxygen at the surface and hydroxyl groups (O_S) (530.9 eV) likely coming from neutralization of ionized oxygen vacancies; and a small percentage of oxygen in C—O bonds (532.4 eV) corresponding to the carbon contamination from the surrounding atmosphere. It should be bear in mind that, obviously, the non-Mg added sample already presents some native defects corresponding to its surface state. Both, titanium and oxygen, are pointing out these features that have strong consequences on the capacity to induce photocatalytic reactions.

In fact, it is plausible to assume that the increase of surface states due to disorder and dopant would enhance visible and infrared absorption, with the additional benefit of photogeneration of carriers. However, this absorption enhancement is too narrow to be significant. UV–vis results (see Supplementary Data Fig. S4) shows that apart from a little shift of the band gap energy to higher values (Supplementary Data Table S1) probably due to higher value of the MgO band gap [45], no significant changes can be appreciated. Then, differences in the photoactivity of the materials are not originated by its different optical properties.

On the contrary, these extended energy states, in combination with the energy levels produced by dopants, can become recombination centres or, alternatively, effective trapping centres. In the former case, which implies the annihilation of photogenerated carriers, they have as a consequence a diminishing on the photocatalytic productivity. In the second case, surface states can capture one of the carriers preventing its direct and rapid recombination and enhancing the possibility to be transferred to the photocatalytic reactions. It is well known that Ti^{3+} acts as an electron trap preventing its recombination with the photogenerated holes and increasing the probability of the photoreduction of the CO_2 chemisorbed molecules [46]. Additionally, the hydroxyl surface groups can act as hole traps [47] to form a new radical which facilitates the oxygen evolution reaction.

The relative abundance of the modified oxygen states (O_S) and reduced titanium (Ti^{3+}) for each Mg loading were calculated as the ratio of the deconvoluted area of the O_S and Ti^{3+} contributions over their corresponding peak area (O_S/O and Ti^{3+}/Ti, respectively). From the plot of this relative abundance in front of Mg loading (Fig. 4), it was found that the sample with the highest O_S and Ti^{3+} contributions was 0.2 wt% Mg. It is arguably that the maximum substitutional incorporation of magnesium is found for this concentration. At higher loadings a stronger influence on the surface distortion happened and, at the same time, not all the magnesium was incorporated into the lattice, in favour to the nucleation of a new intermetallic phase $MgTiO_3$.

3.3. Photocatalytic activity

TiO_2 and Mg–TiO_2 photocatalysts were immobilized over glass substrates and their activity towards carbon dioxide reduction was tested using water as hole scavenger and simulated solar light as energy source. In gas phase reactors, carbon dioxide can be reduced

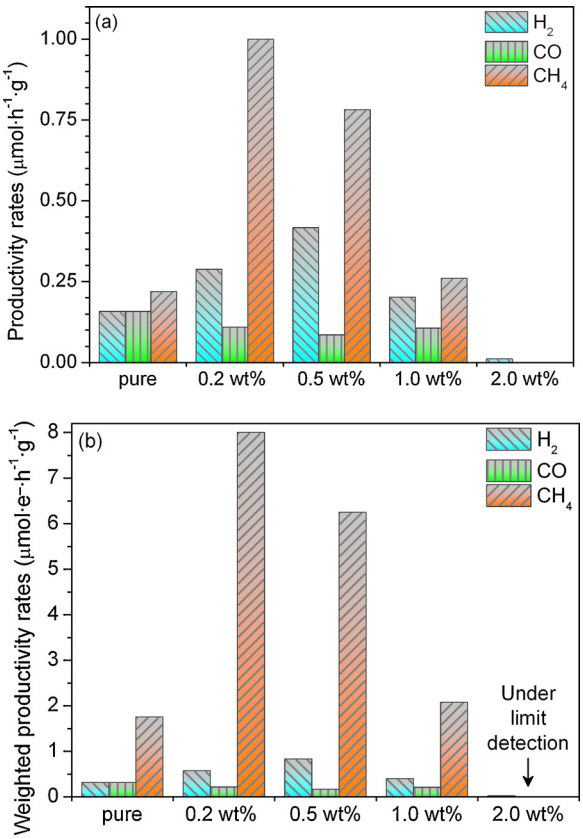

Fig. 5. (a) Averaged CH_4, CO and H_2 productivity rates to CO_2 photoreduction after 3 h of illumination. (b) Weighted productivity rates taking into account the number of electrons involved in the photoreduction reaction, 8 electrons for CH_4 and 2 for H_2 or CO.

to different products, mainly carbon monoxide and methane, processes that are competitive with the hydrogen formation from water reduction. The following reactions can, in a simple way, describe the mechanisms involved in the photoreduction of carbon dioxide, including the photoactivation of the catalyst, water oxidation to O_2, reduction of carbon dioxide to CO or CH_4 and water reduction to H_2:

$$\text{Photogeneration of carriers:} \quad TiO_2 \xrightarrow{h\nu} e^- + h^+ \tag{2}$$

$$\text{Water photooxidation:} \quad 2H_2O + 4h^+ \rightarrow O_2 + 4H^+ \tag{3}$$

$$CO_2 \text{ photoreduction to } CH_4: \quad CO_2 + 8H^+ + 8e^- \rightarrow CH_4 + 2H_2O \tag{4}$$

$$CO_2 \text{ photoreduction to CO:} \quad CO_2 + 2H^+ + 2e^- \rightarrow CO + 2H_2O \tag{5}$$

$$\text{Water photoreduction:} \quad 2H^+ + 2e^- \rightarrow H_2 \tag{6}$$

In this study, CH_4, CO and H_2 were found to be the main products from the CO_2 photoreduction, although other minority by-products were also detected, at the level of the GC analyser resolution, such as C_2H_6 and C_3H_8.

As shown in Fig. 5a, magnesium modified TiO_2 highly enhanced the conversion rates of the photoreduction process, obtaining up to a 3-fold increase in the total productivity. However, as magnesium concentration increases, the overall productivity decreases. Those doped with 0.2 and 0.5 wt% Mg increases the methane yield by 4.5 and 3.5 times with respect to the obtained with pure TiO_2 nanoparticles. Besides, H_2 production was also increased, obtaining approximately twice the amount produced without doping, for 0.5 wt% Mg sample, while the production of CO is slightly reduced.

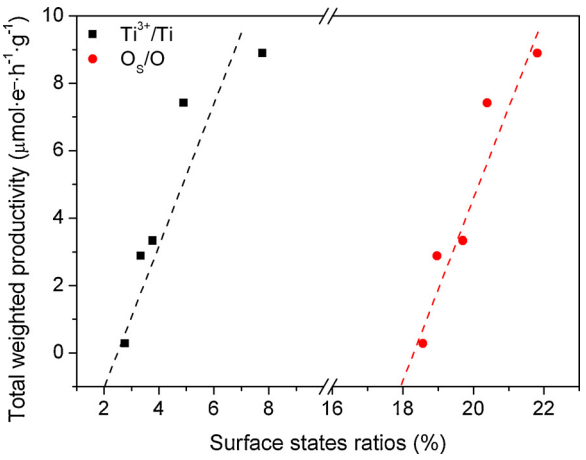

Fig. 6. Dependence of the weighted productivity rates with the relative abundance of defective sites for the different Mg-loaded catalysts.

Then, magnesium incorporation affects both the productivity as well as the selectivity CH_4/H_2 ratio as we will discuss later.

A remarkable picture of the processes taking place at the surface corresponds to the analysis of the productivity considered as the overall number of transferred electrons used for the formation of the analyzed molecules according to the above indicated reactions (Eqs. (4)–(6)), namely weighted productivity (Fig. 5b), as a first approach of quantification of internal quantum efficiency (IQE) of the semiconductor, where it can be highlight that the magnesium incorporation induces a 3-fold increase in its IQE.

Looking at the dependence of the weighted productivity versus the relative abundance of modified oxygen states (O_S) and reduced titanium (Ti^{3+}), shown in Fig. 6, it is clearly seen that the overall productivity shows an excellent correlation with the above mentioned surface states. It is significant that the overall number of available photogenerated carriers to reduce either carbon dioxide or water is not depending of the catalyst additive concentration, but it is rather revealing a strong connection with the chemical structure of the outermost layers through this dependence versus Ti^{3+} and surface oxygen species. Therefore, it can be stated that the magnesium incorporation on titania, apart from changing the acid base properties, promotes a highly modified surface with a major presence of Ti^{3+} and hydroxyl groups, which are responsible for the enhancement on the photoactivity. Nevertheless, more detailed analysis about activity of each type of site, for example Mg or Ti^{3+}, should be done in order to elucidate which is the individual contribution of each site to the productivity of the process.

Additionally, it is noticeable that there is a direct competition between the hydrogen and methane formation whereas the formation of CO appears to be residual. Whereas for 0.2 wt% Mg sample the CH_4/H_2 weighted productivity ratio is about 14, it decreases to 7 for 0.5 wt% Mg and to around 5 at concentrations of 1.0 wt% Mg, which is almost the same value than for pure TiO_2 (see Supplementary Data, Fig. S3). At the same time, global productivity decreases and the hydrogen production becomes more effective likely due to a less favourable chemisorption of CO_2, which is probably caused for the diminution of Ti^{3+}. Due to the electronegativity and the Lewis acid strength of Ti^{3+}, CO_2 is favourably bonded on Ti^{3+} sites than Ti^{4+} sites. Additionally, magnesium is known to contribute in a number of CO_2 involving reactions, including carbon dioxide hydrogenation, by stabilization of CO_2 at the surface of the catalyst allowing a later hydrogenation to form methane instead of other byproducts. DFT and TPD studies revealed that the absorption of CO_2 is not favourable over MgO stable facets [48], whereas for less stable facets CO_2 is strongly bonded. Then, the selectivity to methane can be attributed to that either the increased Ti^{3+} concentration or the

substitutional magnesium on titanium lattice, which is less stable than $MgTiO_3$ phase, promotes the stabilization of CO_2 at the surface allowing its complete reduction, probably via dissociated hydrogen as it was pointed out in literature [35].

The highly dependence of the overall productivity on the Ti^{3+} and O_S suggests that the electron and hole transfer is mediated by surface states.

On one hand, it is known that, in the water splitting process, the rate limiting step of the overall reaction is the photooxidation of water [49] since it involves 4 holes requiring a longer lifetime of carriers than that of the required for the reduction of water. Similarly, in carbon dioxide photoreduction in presence of water, this reaction is also required (Eq. (3)), since the introduction of water into the reactor serves as hole scavenger. Thus, it is plausible that, according to the kinetic data obtained, the hydroxyl groups at the surface may play an important role for the transference of the four required holes.

On the other hand, photogenerated electrons have been found to present a high competition among three different via: (i) direct recombination with holes, (ii) trapping by the Ti^{3+} centres and transfers to the CO_2 molecules and (iii) direct transfer from the conduction band for the reduction of the water molecule. Thus, Ti^{3+} sites play the role of electron trap centres avoiding recombination, enhancing the charge transfer involved in the reduction as well as promoting the CO_2 chemisorption, together with magnesium. This essential role of Ti^{3+} in the photocatalytic activity of titania has already been reported in the literature [46]. Additionally, thermal programmed desorption (TPD) analysis using CO_2 as probe molecule have shown that Ti^{3+} sites bind CO_2 more strongly than Ti^{4+} sites. Then, the time of residence of the adsorbed molecules would rise, increasing the probability that the reaction occurs.

4. Conclusions

In this work, the role played in the photocatalytic activity towards CO_2 photoreduction by the outermost layers of bare and Mg-loaded TiO_2 nanoparticles has been discussed. It has been found that small amount of Mg-loading promotes an increase of the Ti^{3+} (electron trap) and O_S (hole trap) concentration, maintaining a low electron-hole recombination rate according to the considerable increase of the productivity (up to 3 times for 0.2 wt% loaded additive). However, surface instability rises suddenly as additive concentration increases, resulting in a fast decrease of the productivity as the surface recombination increases and, simultaneously, to a less competitive pathway for the CO_2 reduction as proportionally the production of hydrogen is increased in comparison with that of the methane. In fact, a straightforward correlation between the total productivity obtained from the photocatalytic process and the density of Ti^{3+} and O_S has been stated, revealing and corroborating the outstanding significance of the surface chemical structure. Changing the chemical structure of the outermost layers plays the determinant role of the photocatalytic functional behaviour.

Acknowledgements

We thank Dr. Ignasi Salvadó for his earlier contributions to this work. This work was supported by Carburos Metálicos, Air Products group, as part of the CENIT SOST-CO2 project, co-financed by Ministerio de Economía y Competitividad-CDTI CEN2008-1027. Additional support from the Ministerio de Economia y Competitividad by projects CSD2009-00050, MAT 2010-21510, ENE2012-3651 and the European Regional Development Funds (ERDF, "FEDER Programa Competitivitat de Catalunya 2007–2013") was also provided.

Appendix A. Supplementary data

Supplementary data associated with this article can be found, in the online version, at http://dx.doi.org/10.1016/j.apcatb.2013.11.036.

References

[1] A. Goeppert, M. Czaun, G.K. Surya Prakash, G.A. Olah, Energy Environ. Sci. 5 (2012) 7833–7853.
[2] M. Aresta, A. Dibenedetto, Dalton Trans. (2007) 2975–2992.
[3] G.A. Olah, A. Goeppert, G.K.S. Prakash, J. Org. Chem. 74 (2008) 487–498.
[4] T. Inoue, A. Fujishima, S. Konishi, K. Honda, Nature 277 (1979) 637–638.
[5] M. Subrahmanyam, S. Kaneco, N. Alonso-Vante, Appl. Catal. B 23 (1999) 169–174.
[6] J.C.S. Wu, H.-M. Lin, C.-L. Lai, Appl. Catal. A 296 (2005) 194–200.
[7] O.K. Varghese, M. Paulose, T.J. LaTempa, C.A. Grimes, Nano Lett. 9 (2009) 731–737.
[8] C.-C. Yang, J. Vernimmen, V. Meynen, P. Cool, G. Mul, J. Catal. 284 (2011) 1–8.
[9] N.Z. Muradov, T.N. Veziroğlu, Int. J. Hydrog. Energy 33 (2008) 6804–6839.
[10] R.C. Baliban, J.A. Elia, V. Weekman, C.A. Floudas, Comput. Chem. Eng. 47 (2012) 29–56.
[11] P.T. Anastas, M.M. Kirchhoff, Acc. Chem. Res. 35 (2002) 686–694.
[12] B.J.M. de Vries, D.P. van Vuuren, M.M. Hoogwijk, Energy Policy 35 (2007) 2590–2610.
[13] P. Anastas, N. Eghbali, Chem. Soc. Rev. 39 (2010) 301–312.
[14] F. Raimondi, G.G. Scherer, R. Kötz, A. Wokaun, Angew. Chem. Int. Ed. 44 (2005) 2190–2209.
[15] X. Chen, S.S. Mao, Chem. Rev. 107 (2007) 2891–2959.
[16] O. Ozcan, F. Yukruk, E.U. Akkaya, D. Uner, Appl. Catal. B: Environ. 71 (2007) 291–297.
[17] T.-V. Nguyen, J.C.S. Wu, C.-H. Chiou, Catal. Commun. 9 (2008) 2073–2076.
[18] M. Hamadanian, A. Reisi-Vanani, A. Majedi, Mater. Chem. Phys. 116 (2009) 376–382.
[19] S. In, A. Orlov, R. Berg, F. Garcia, S. Pedrosa-Jimenez, M.S. Tikhov, D.S. Wright, R.M. Lambert, J. Am. Chem. Soc. 129 (2007), 13790-+.
[20] X. Chen, L. Liu, P.Y. Yu, S.S. Mao, Science 331 (2011) 746–750.
[21] H. Zuoli, Q. Wenxiu, X. Haixia, C. Jing, Y. Yuan, S. Peng, J. Am. Ceram. Soc. 95 (2012) 3941–3946.
[22] K. Koci, L. Obalova, Z. Lacny, Chem. Pap. 62 (2008) 1–9.
[23] A. Valdes, J. Brillet, M. Gratzel, H. Gudmundsdottir, H.A. Hansen, H. Jonsson, P. Klupfel, G.-J. Kroes, F. Le Formal, I.C. Man, R.S. Martins, J.K. Norskov, J. Rossmeisl, K. Sivula, A. Vojvodic, M. Zach, PCCP 14 (2012) 49–70.
[24] Z. Bian, T. Tachikawa, W. Kim, W. Choi, T. Majima, J. Phys. Chem. C 116 (2012) 25444–25453.
[25] I. Paramasivam, H. Jha, N. Liu, P. Schmuki, Small 8 (2012) 3073–3103.
[26] U. Diebold, Surf. Sci. Rep. 48 (2003) 53–229.
[27] J. Bandara, C.C. Hadapangoda, W.G. Jayasekera, Appl. Catal. B 50 (2004) 83–88.
[28] N. Venkatachalam, M. Palanichamy, B. Arabindoo, V. Murugesan, Catal. Commun. 8 (2007) 1088–1093.
[29] L. Liu, C. Zhao, H. Zhao, D. Pitts, Y. Li, Chem. Commun. 49 (2013) 3664–3666.
[30] S. Xie, Y. Wang, Q. Zhang, W. Fan, W. Deng, Y. Wang, Chem. Commun. 49 (2013) 2451–2453.
[31] R.D. Shannon, Acta Crystallogr. Sect. A 32 (1976) 751–767.
[32] R.G. Pearson, J. Am. Chem. Soc. 85 (1963) 3533–3539.
[33] C. Fàbrega, T. Andreu, A. Cabot, J.R. Morante, J. Photochem. Photobiol. A 211 (2010) 170–175.
[34] C.-C. Yang, Y.-H. Yu, B. van der Linden, J.C.S. Wu, G. Mul, J. Am. Chem. Soc. 132 (2010) 8398–8406.
[35] D. Uner, M.M. Oymak, Catal. Today 181 (2012) 82–88.
[36] Y. Li, S. Peng, F. Jiang, G. Lu, S. Li, J. Serb. Chem. Soc. 72 (2007) 393–402.
[37] Y. Suzuki, Y. Shinoda, Sci. Technol. Adv. Mater. 12 (2011).
[38] A.M. Ruiz, G. Dezanneau, J. Arbiol, A. Cornet, J.R. Morante, Chem. Mater. 16 (2004) 862–871.
[39] A.M. Ruiz, G. Sakai, A. Cornet, K. Shimanoe, J.R. Morante, N. Yamazoe, Sens. Actuators B 93 (2003) 509–518.
[40] F. Liu, L. Lu, P. Xiao, H. He, L. Qiao, Y. Zhang, Bull. Korean Chem. Soc. 33 (2012) 2255–2259.
[41] S. Na-Phattalung, M.F. Smith, K. Kim, M.-H. Du, S.-H. Wei, S.B. Zhang, S. Limpijumnong, Phys. Rev. B 73 (2006) 125205.
[42] M.C. Biesinger, B.P. Payne, A.P. Grosvenor, L.W.M. Lau, A.R. Gerson, R.S.C. Smart, Appl. Surf. Sci. 257 (2011) 2717–2730.
[43] E. McCafferty, J.P. Wightman, Surf. Interface Anal. 26 (1998) 549–564.
[44] J.G. Yu, X.J. Zhao, Q.N. Zhao, Thin Solid Films 379 (2000) 7–14.
[45] D.M. Roessler, W.C. Walker, Phys. Rev. 159 (1967) 733–738.
[46] K. Suriye, P. Praserthdam, B. Jongsomjit, Appl. Surf. Sci. 253 (2007) 3849–3855.
[47] T.L. Villarreal, R. Gámez, M. Neumann-Spallart, N. Alonso-Vante, P. Salvador, J. Phys. Chem. B 108 (2004) 15172–15181.
[48] H.Y. Kim, H.M. Lee, J.-N. Park, J. Phys. Chem. C 114 (2010) 7128–7131.
[49] J. Tang, J.R. Durrant, D.R. Klug, J. Am. Chem. Soc. 130 (2008) 13885–13891.